Bose-condensate tunneling dynamics: Momentum-shortened pendulum with damping

I. Marino,[1] S. Raghavan,[1,2] S. Fantoni,[1,3] S. R. Shenoy,[1] and A. Smerzi[3]
[1]*Abdus Salam International Centre for Theoretical Physics, I-34100 Trieste, Italy*
[2]*Rochester Theory Center for Optical Science and Engineering, Department of Physics and Astronomy, University of Rochester, Rochester, New York 14627*
[3]*Istituto Nazionale de Fisica della Materia and International School for Advanced Studies, via Beirut 2/4, I-34014 Trieste, Italy*
(Received 20 November 1998)

Bose-Einstein condensates in a double-well trap, as well ^{3}He-B baths connected by micropores, have been shown to exhibit Josephson-like tunneling phenomena. Unlike the superconductor Josephson junction of phase difference ϕ that maps onto a rigid pendulum of energy $\cos(\phi)$, these systems map onto a momentum-shortened pendulum of energy $-\sqrt{1-p_\phi^2}\cos(\phi)$ and length $\sqrt{1-p_\phi^2}$, where p_ϕ is a population imbalance between the wells/baths. We study here the effect of damping on the four distinct modes of the nonrigid pendulum, characterized by distinct temporal mean values, $\langle\phi\rangle$ and $\langle p_\phi\rangle$. Damping is shown to produce different decay trajectories to the final equilibrium $\phi=0=p_\phi$ state that are characteristic dynamic signatures of the initial oscillation modes. In particular, damping causes π-state oscillations with $\langle\phi\rangle=\pi$ to increase in amplitude and pass through phase-slip states, before equilibrating. Similar behavior has been seen in ^{3}He-B experiments. [S1050-2947(99)03207-2]

PACS number(s): 03.75.Fi, 74.50.+r, 05.30.Jp, 32.80.Pj

I. INTRODUCTION

Phase coherent Bose-Einstein condensates (BEC) have recently been observed in systems of alkali-metal atoms [1]. The superfluidity of these condensates, however, can only be verified through some characteristic signatures like the presence of persistent Josephson tunneling currents [2–8]. These Josephson-like phenomena, as well as richer oscillation modes, have been predicted in double-well magnetic traps, and between two condensates in different hyperfine levels [3–8]. Some of these effects have experimentally been observed in a vertical array of trapped Bose-Einstein condensates [10] and in ^{3}He-B baths connected by micropores [11], including metastable states with a phase difference of π [5,6,9] between baths [11].

Mechanical analogues have been useful in providing a physical understanding of superconducting Josephson junctions (SJJ) [12,13]. These include a pendulum analog where the tilt angle ϕ is the phase difference across the junction; the angular momentum p_ϕ is the junction voltage; the pendulum length is the Josephson critical current; and the moment of inertia and pendulum damping are the junction capacitance and shunt resistance. With circuit inductance, the analog has an added torsion bar, introducing an additional tilt angle. In all SJJ cases, however, the pendulum is rigid, with length independent of the state of the system.

By contrast, the BEC [5,6] and ^{3}He-B [9] atomic tunnel junctions map onto a *nonrigid* pendulum, with length dependent on the canonical momentum as $\sim\sqrt{1-p_\phi^2}$: ''faster equals shorter.'' This means that the oscillation modes are richer than those of the rigid pendulum.

In this paper, we investigate the effects of damping on the nonrigid-pendulum oscillation modes of tunneling BEC. The central result is that each mode has a unique dynamical trajectory to the common final $\langle\phi\rangle=0=\langle p_\phi\rangle$ rest state that is thus a characteristic mode signature.

Section II outlines the five characteristic oscillation modes of the momentum-shortened pendulum without damping. Section III adds damping through $\dot\phi$, the angular velocity, showing how the p_ϕ-ϕ phase space and pendulum coordinate locii are affected. Finally, Sec. IV presents our conclusions.

II. NONRIGID PENDULUM WITHOUT DAMPING

We now briefly summarize the derivation of the boson Josephson junction dynamical equations at temperature $T=0$ derived in [5,6]. Bose-Einstein condensates, with wave function $\Psi(r,t)$, obey, within a mean-field approximation, a Gross-Pitaevskii equation (GPE) [2]. Josephson-like tunneling has been predicted between two BEC populations in double-well traps [2–8]. To describe such tunneling, we approximate the wave function with $N_{1,2}$ atoms in traps 1,2 by a linear combination of time-independent single-well (normalized to unity) wave functions $\Phi_{1,2}(r,\frac{1}{2}N_T)$,

$$\Psi(r,t)=\psi_1(t)\,\Phi_1(r,\tfrac{1}{2}N_T)+\psi_2(t)\,\Phi_2(r,\tfrac{1}{2}N_T). \quad (2.1)$$

Here $N_1(t)+N_2(t)=N_T$ is a constant, and the complex amplitudes are defined by $\psi_{1,2}(t)=e^{i\theta_{1,2}(t)}|\psi_{1,2}(t)|$, with $N_{1,2}(t)\equiv|\psi_{1,2}(t)|^2$. Integrating over spatial coordinates yields coupled dynamic equations for the amplitudes,

$$i\hbar\dot\psi_1=E_1\psi_1+U_1|\psi_1|^2\psi_1-K\psi_2, \quad (2.2a)$$

$$i\hbar\dot\psi_2=E_2\psi_2+U_2|\psi_2|^2\psi_2-K\psi_1. \quad (2.2b)$$

Here $E_{1,2}$ are the zero point energies for wells 1,2 (determined by the trap curvatures); $U_{1,2}$ are proportional to the mean-field energy; K is determined by the off-diagonal matrix elements of the trap potentials and kinetic energies between $\Phi_{1,2}(r;\frac{1}{2}N_T)$ wave functions, yielding tunneling be-

tween wells. The parameters $E_{1,2}$, U, and K are independent of $[N_1(t)-N_2(t)]$ in this approximation, and are only dependent on the fixed N_T.

Defining the relative phase difference $\phi \equiv \theta_2 - \theta_1$, and the fractional population imbalance $z \equiv (N_1 - N_2)/N_T$, Eqs. (2.2) for $\psi_{1,2}$ can be rewritten in terms of those variables as

$$\dot{z} = -\sqrt{1-z^2}\sin\phi, \tag{2.3a}$$

$$\dot{\phi} = \Lambda z + \Delta E + \frac{z}{\sqrt{1-z^2}}\cos\phi. \tag{2.3b}$$

These equations describe the dynamics of the boson Josephson junction (BJJ) [5,6]. The right-hand side of Eq. (2.3b) gives the chemical potential difference through $\Delta\mu = -\hbar\,\dot{\phi}$. Here $\Lambda \equiv (U_1+U_2)N_T/4K$, $\Delta E \equiv (E_1-E_2)/2K + (U_1 - U_2)N_T/4K$, and the time is scaled in $2K/\hbar$. Equations (2.3) imply that z is the conjugate momentum for the generalized (angular) coordinate ϕ, with system Hamiltonian

$$H = \tfrac{1}{2}\Lambda z^2 + \Delta E z - \sqrt{1-z^2}\cos\phi. \tag{2.4}$$

This allows us to identify the population imbalance z, with the canonical momentum p_ϕ mentioned in the Introduction, giving the pendulum modes their physical significance.

Superconductor Josephson junctions have been phenomenologically modeled by Schrödinger-like equations similar to Eqs. (2.2) [13,14] (without the nonlinear term). One obtains a Josephson coupling energy proportional to $-\sqrt{N_1 N_2}\cos\phi$, but as charge leakages through the external circuit strongly suppress population imbalances, then $N_1 = N_2 = \frac{1}{2}N_T$ and $z \approx 0$ [15]. This SJJ coupling energy $\sim -\cos\phi$ is thus that of a *rigid* pendulum, with all junction oscillation modes (including those with circuit inductance [12]) being those of the rigid-pendulum analogy. Comparing with Eqs. (2.4), we see that the BJJ of charge-neutral atoms is described in general by a *nonrigid* momentum-shortened pendulum of length $\sqrt{1-z^2}$, where z is a canonical momentum [5,6].

^{3}He-B baths connected by micropores [11] that act as Cooper-pair tunneling barriers can also be shown to map onto a nonrigid pendulum, with ϕ the BCS gap phase difference, and z the number difference in a region of depressed order parameter, just outside the micropore [9].

The oscillation modes of the momentum-shortened nonrigid pendulum are of five types [5,6], distinguished by mean values of $\langle\phi\rangle, \langle z\rangle$ of the tilt angle and angular momentum. As shown in Fig. 1(a) these are (A) ''zero-phase'' oscillations about the downward-orientation rest position, with $\langle\phi\rangle = \langle z\rangle = 0$; (B) ''running-phase'' pendulum rotations of phase $-\infty < \phi < \infty$, with nonzero angular momentum $\langle z\rangle \neq 0$, corresponding to a ''macroscopic quantum self-trapping'' of nonzero, self-maintained value of the population imbalance; (C) ''π-phase'' oscillations about the vertical upward-oriented pendulum, $\langle\phi\rangle = \pi$, with $\langle z\rangle = 0$, nonself-trapping; and (D) ''π-phase'' rotations of the inverted pendulum, but with a closed trajectory of temporal averages $\langle z\rangle \neq 0$ (corresponding to π self-trapping) in the inverted $\langle\phi\rangle = \pi$ orientation. (There are two different kinds of such self-trapped π states $\langle z\rangle < z$, and $\langle z\rangle > z \equiv \sqrt{1-1/\Lambda^2}$.)

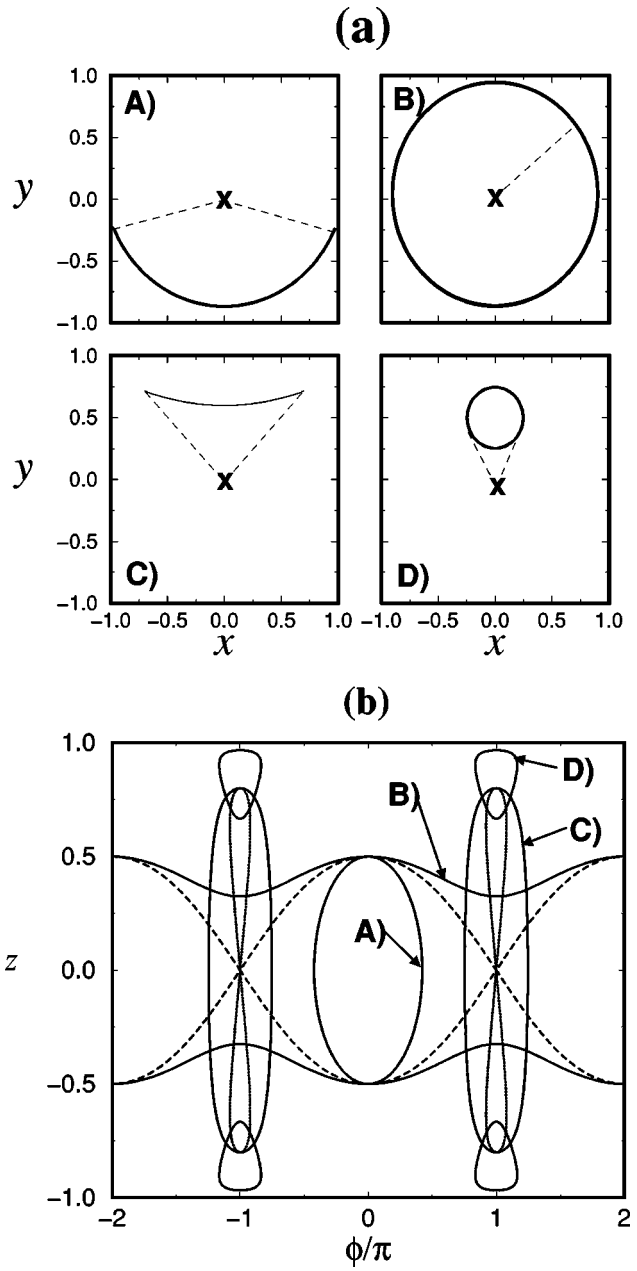

FIG. 1. (a) Plots of (dimensionless) coordinate-space locii (x,y) nonrigid undamped pendulum, for types of oscillation modes described in the text. The parameters, average, and initial phase/momentum variables are (A) $\Lambda = 5$; $\langle\phi\rangle = 0 = \langle z\rangle$; $z(0) = 0.5$, $\phi(0) = 0$; (B) $\Lambda = 25$; $-\infty < \langle\phi\rangle < \infty$, $\langle z\rangle = 0.5$; $z(0) = 0.5, \phi(0) = 0$; (C) $\Lambda = 0.36$; $\langle\phi\rangle = \pi$, $\langle z\rangle = 0$; $z(0) = 0.8$, $\phi(0) = \pi$; (D) $\Lambda = 2$; $\langle\phi\rangle = \pi$, $\langle z\rangle = 0.866$; $z(0) = 0.666$, $\phi(0) = \pi$. The cross represents the pendulum support, the dashed lines are particular pendulum lengths; (b) phase-space z-ϕ plots for the undamped nonrigid pendulum, showing the five types of oscillations as given in the text, for the cases (A)–(D) in (a). The dashed line represents the separatrix between bounded and self-trapped motions for $\langle\phi\rangle = 0$, and the dotted line represents the separatrix of the bounded and self-trapped motions for $z(0) = 0.8$ and $\langle\phi\rangle = \pi$.

The $z(t)$, $\phi(t)$ time variations have been presented previously, and are exactly soluble in terms of elliptic functions [5,6]. The spatial coordinates $(x,y) = (\sqrt{1-z^2}\sin\phi, -\sqrt{1-z^2}\cos\phi)$ of the pendulum clearly show these different modes as distinctive pendulum locii, as in Fig. 1(a). BJJ

modes (A) and (B) have analogies with the SJJ rigid pendulum (although the physical variables are quite different). However, modes (C) and (D) are peculiar to the momentum-shortened pendulum. Note that the nonrigid pendulum is shortest at the bottom of its swing, so the locus of Fig. 1(a) is flatter than that of the rigid-pendulum unit circle. This length variation is crucial to enabling the π states of (C) and (D) to exist. (B) and (D) correspond to pendulum modes of nonzero angular momentum $\langle z\rangle \neq 0$, with closed-loop trajectories enclosing the pendulum support point for running mode (B); but lying above for the self-trapped π-state rotation.

As parameters Λ, ΔE are varied, for given initial conditions $z(0), \phi(0)$, one can have transitions between $\langle z\rangle = 0$ states and self-trapped states with $\langle z\rangle \neq 0$, with the inverse oscillation period falling to zero at critical parameter values [5,6]. In Fig. 1(b) we show the nonrigid-pendulum phase portrait (for $\Delta E = 0$). The solid lines are constant-energy contours for initial conditions as in Fig. 1(a). Linearizing about $\phi = 0 = z$, the small-amplitude angular dimensionless frequencies are $\omega_0 = \sqrt{1+\Lambda}$. The heavy dashed line is a separatrix at a critical $\Lambda = \Lambda_c = [1 + \sqrt{1-z^2(0)}\cos\phi(0)]/(z^2(0)/2)$, where the inverse period dips to zero [5,6], and beyond which the running-phase (B) oscillation sets in. Linearizing around $\phi = \pi, z = 0$, small-amplitude π-phase (C) oscillations are of angular frequency $\omega_\pi = \sqrt{1-\Lambda}$, with $\Lambda < 1$. The heavy dotted line is a separatrix, when the contours pinch off at $z = 0, \phi = \pi$, and beyond which two separate contours with $\langle z\rangle \neq 0$ emerge, for the π-phase (D) rotations.

It is also possible to plot constant-energy contours for fixed Λ, and a variety of initial conditions for the four different modes described above. In this case, it is found that for mode (A), contours of decreasing energy have decreasing amplitude. However, for modes (C) and (D), decreasing-energy contours have increasing amplitude. This observation will become relevant in the next section when we try to understand the effects of damping. We now examine the damped nonrigid-pendulum trajectories in more detail.

III. NONRIGID PENDULUM WITH DAMPING

The first question to ask is what form the damping term should have in the equations of motion. This problem has been addressed in [4], where it has been assumed that, for BEC, there will be a noncoherent dissipative current of normal-state atoms, or Bogoliubov quasiparticles, proportional to the chemical potential difference $\Delta\mu$ [4]. This dissipative current is the analog of the normal current branch in a single Josephson junction, $I_d = -G\,\Delta\mu$, with G the dc conductance. The equations for the BEC model damped nonrigid pendulum are then

$$\dot{z} = -\sqrt{1-z^2}\sin\phi - \eta\dot{\phi}, \tag{3.1a}$$

$$\dot{\phi} = \Lambda\, z + \Delta\, E + \frac{z}{\sqrt{1-z^2}}\cos\phi, \tag{3.1b}$$

where $\eta \equiv 2\hbar G/N_T$ is a dimensionless damping constant.

To be in the underdamped regime for zero-phase oscillations, the damping contribution to the linearized form of Eqs. (3.1) ($\Delta E = 0$),

$$\ddot{\phi} + (1+\Lambda)\,\phi + \eta(1+\Lambda)\,\dot{\phi} \approx 0, \tag{3.2}$$

must be small, i.e., $\eta\sqrt{1+\Lambda} \ll 1$. This ratio has been estimated [4] to be of order ~ 0.5–0.04. This is exponentially reduced further, for lower temperatures; however, we will use a moderate damping parameter value $\eta = 0.05$ in most plots of numerical solutions of Eqs. (3.1), in order to more clearly display the decaying trajectories under damping.

Although we focus here on the double-well BEC damping as in Eqs. (3.1) through the angular velocity, $\dot{z} \sim -\eta\,\dot{\phi}$, other two-state systems such as two condensates in different hyperfine levels in a single harmonic trap, connected by ''tunneling'' transitions [8], can have damping from the finite lifetime of excited states. This appears through the angular momentum, $\dot{z} \sim -\eta\, z$ (that is not just proportional to the angular velocity) [16].

We first consider damping for the symmetric-well case $\Delta E = 0$. The final asymptotic state reached, for all $z(0), \phi(0), \Lambda$ values, is the downward-oriented pendulum at rest, $\phi = 0 = z$, as is physically reasonable. However, the way in which this equilibrium state is reached is different for all four oscillation modes: the different trajectories constitute the distinct dynamical signatures of the oscillation modes themselves. We consider each of these in turn.

(A) *Zero-phase mode*, $\langle\phi\rangle = 0 = \langle z\rangle$. Figure 2(a) shows the locus of the nonrigid-pendulum (x,y) coordinates with $\phi(0) = 0$, $z(0) = 0.5$, $\Lambda = 5$, and $\eta = 0.05$. Clearly, there is damping down to the rest state, with increasing length and decreasing amplitude. Figure 2(b) shows the same behavior in z-ϕ phase space, with inward spiraling contours of decreasing energy. The maximum (dimensionless) frequency attained, from Eq. (3.2), is

$$\omega_0(\Lambda,\eta) = \sqrt{1+\Lambda-\tfrac{1}{4}\eta^2\,(1+\Lambda)^2} \tag{3.3}$$

and the system quickly damps to this low-amplitude regime when exponential decay sets in, with characteristic damping time

$$\tau_0(\Lambda,\eta) = \frac{2}{\eta\,(1+\Lambda)}. \tag{3.4}$$

(B) *Running-phase mode*, $\langle z\rangle \neq 0$. Figure 3(a) shows the locus of the nonrigid-pendulum coordinates with $\Lambda = 25$, and all other parameters and initial conditions as before. Starting with rotation of nonzero angular momentum as in Fig. 1(b), the coordinate-space trajectory damps smoothly to $\langle z\rangle = 0$ oscillations and finally settles to the rest state. The phase-space z-ϕ trajectory of Fig. 3(b) shows this z decrease and capture by one of the $\phi = 2n\pi$ energy potential minima.

It has been shown [5,6] for zero damping, $\eta = 0$, that the inverse oscillation period $\omega_0(\Lambda,0)$ dips to zero as Λ is increased through a critical $\Lambda = \Lambda_c$, at the onset of a ''self-trapped'' state. With a characteristic frequency $\omega_0(\Lambda,\eta)$ in the $\eta \neq 0$ damped case, defined from the highest peak of the power spectrum $|z(\omega)|^2$, we find that a dip at $\Lambda_c = \Lambda_c(\eta)$ persists, but no longer to zero. This is seen in Fig. 3(c).

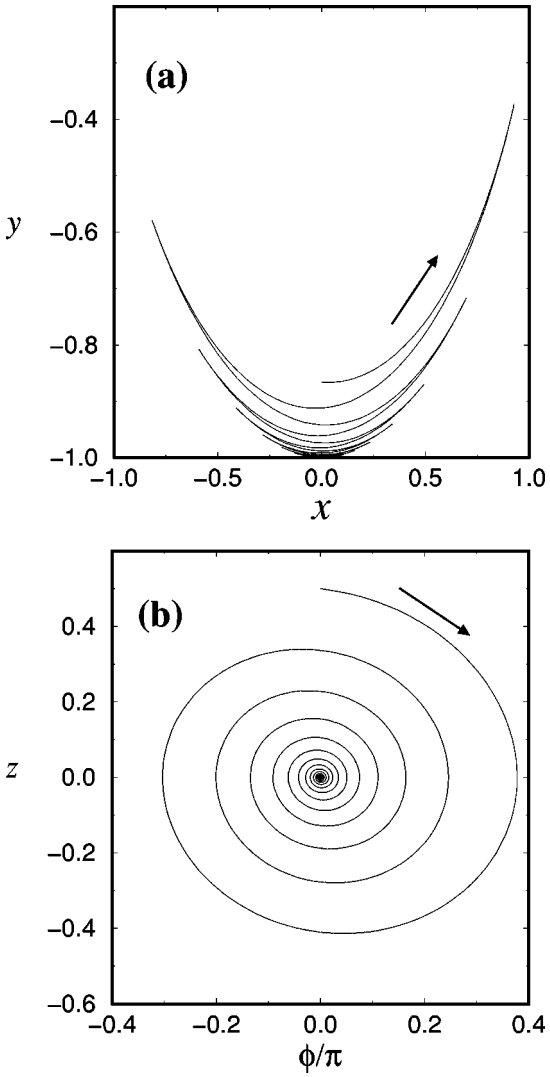

FIG. 2. (a) Nonrigid-pendulum coordinate-space trajectory, for mode (A) of Fig. 1, $\phi(0)=0$, $z(0)=0.5$, and damping $\eta=0.05$; (b) nonrigid-pendulum phase-space trajectory for mode (A) of Fig. 1, $\phi(0)=0$, $z(0)=0.5$, and damping $\eta=0.05$.

We next consider the damping of π states with average phase $\langle\phi\rangle=\pi$.

(C) *π-phase oscillations with $\langle\phi\rangle=\pi,\langle z\rangle=0$.* Figure 4(a) shows the coordinate-space (x,y) trajectory of the nonrigid-pendulum bob with initial values $\phi(0)=\pi$, $z(0)=0.01$, $\Lambda=0.36$, and damping $\eta=0.05$. Clearly, the system, initially at the top of the figure, starts to oscillate with *increasing* amplitude, with momentum rising and length $\sqrt{1-z^2}$ falling, until z is driven towards unity (zero pendulum length). Since this means that the number of atoms in one well falls below the minimum number needed to sustain a well-defined mean condensate wave function, the semiclassical approximation implicit in Eqs. (2.3) and (3.1) starts breaking down, and quantum fluctuations start becoming important. Numerically, this is signaled as a singularity in Eqs. (3.1), and the onset of a *phase-slip process* (with ϕ jumping by π). We use the interpolation substitution $\sqrt{1-z^2}\rightarrow[(1-z^2)^2+\epsilon]^{1/4}$, where $\epsilon\ll 1$ to follow the behavior of the system past the singularity, although z can then attain unphysical values exceeding unity at some points in the trajectory.

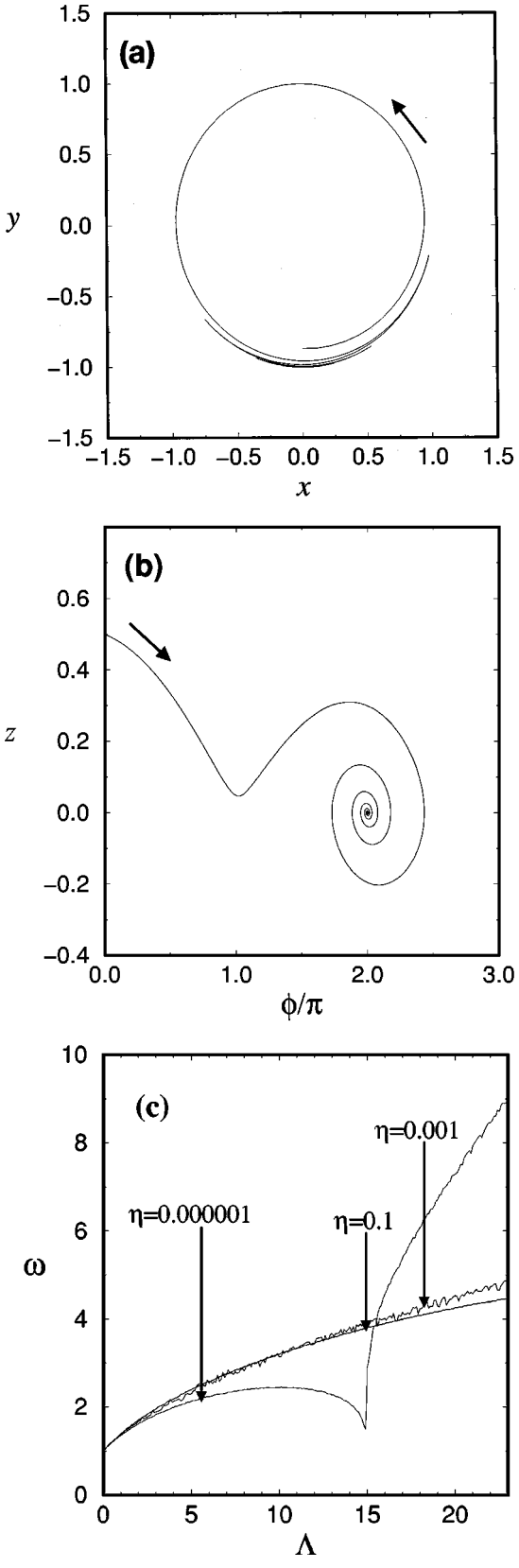

FIG. 3. (a) Coordinate-space trajectory for mode (B) of Fig. 1, and damping $\eta=0.05$; (b) phase-space trajectory for motion shown in (a); (c) oscillation frequency of mode versus inverse mass Λ for $z(0)=0.5$, $\phi(0)=0$, and various dampings $\eta=0.1,10^{-3},10^{-6}$.

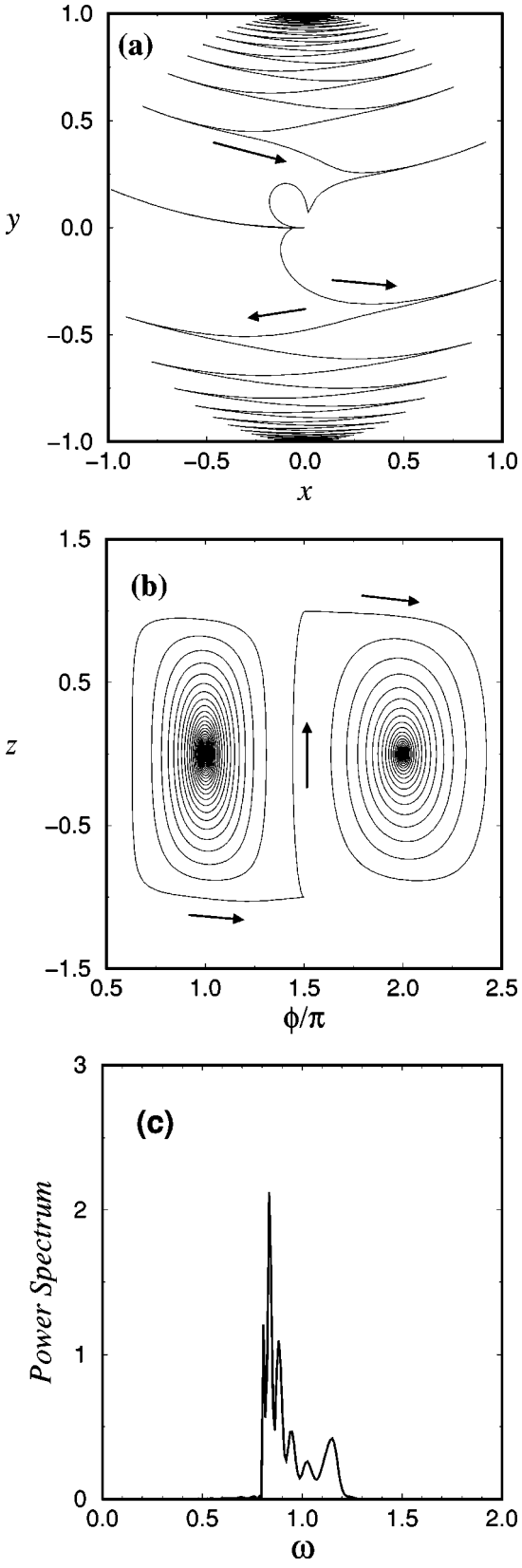

FIG. 4. (a) Coordinate-space trajectory for mode (C) of Fig. 1, with $z(0)=0.01$, and $\eta=0.05$; (b) phase-space trajectory for motion shown in (a); (c) power spectrum $|z(\omega)|^2$ of the momentum versus frequencies explored during the motion depicted in (a),(b).

After the phase slip, the pendulum settles to a final state $\langle\phi\rangle=0$ that damps to rest with decreasing amplitude, as previously stated.

The phase portrait is displayed in Fig. 4(b). The average value of the momentum is $\langle z\rangle=0$. The damped phase-space trajectories spiral outwards, lowering their energies. The amplitudes increase exponentially, with time scales

$$\tau_\pi(\Lambda,\eta)=\frac{2}{\eta(1-\Lambda)} \tag{3.5}$$

as determined by linearizing Eqs. (3.1) about $\phi=\pi, z=0$. The frequency shifts from a minimum initial value

$$\omega_\pi(\Lambda,\eta)=\sqrt{1-\Lambda-\tfrac{1}{4}\eta^2(1-\Lambda)^2} \tag{3.6}$$

to larger frequencies. After a phase slip around $\phi=3\pi/2$, the system settles into a state with $\langle\phi\rangle=2\pi$, equivalent to the zero state, with frequency approaching $\omega_0(\Lambda,\eta)$ of Eq. (3.3), as the pendulum damps with decreasing amplitudes. Figure 4(c) shows the broad spectrum $|z(\omega)|^2$ of frequencies explored during the trajectory, spanning this range $\omega_\pi(\Lambda,\eta)\leqslant\omega\leqslant\omega_0(\Lambda,\eta)$.

(D) *π-phase rotations*, $\langle\phi\rangle=\pi, \langle z\rangle\neq 0$. Figure 5(a) shows in coordinate space the π-state initial pendulum rotation from $\phi(0)=\pi$, $z(0)=0.666$ (which is just slightly smaller than the fixed point value $z_s=\sqrt{1-1/\Lambda^2}$), with $\Lambda=2$, and $\eta=0.05$. Linearizing about $\phi=\pi$, $z=z_s$, the initial frequency of the self-trapped (ST) π state is

$$\psi_\pi^{\mathrm{ST}}(\Lambda,\eta)=\sqrt{\Lambda^2-1-\tfrac{1}{4}\eta^2\Lambda^2(\Lambda^2-1)^2}. \tag{3.7}$$

The trajectory spirals outwards with increasing amplitude, goes through a phase slip, and then damps down with decreasing amplitude to a zero-state oscillation that goes eventually to rest. The phase-space trajectory is given in Fig. 5(b). Comparing with Fig. 3(a), we see that the $\langle z\rangle\neq 0$ state persists until the phase slip occurs in this self-trapped BEC state. The damping-induced initial exponential increase now has the time scale

$$\tau_\pi^{\mathrm{ST}}(\Lambda,\eta)=\frac{2}{\eta\Lambda(\Lambda^2-1)}. \tag{3.8}$$

The $\langle z\rangle>z_s$ state (not shown) goes to a running state, then a zero state.

Thus, Figs. 2–5 for the various oscillation trajectories of the damped nonrigid pendulum depict the distinct dynamical signatures of the different oscillation modes that can be initially set up in the double-well BJJ. For ^{3}He-B tunneling through micropores [11], flows outside the pores introduce an additional ''hydrodynamic'' twist: the total phase difference is not just the phase difference across the pores. (This corresponds to inductive effects in a SJJ, modeled by a torsion bar attached to the pendulum [12].) However, we expect coordinate- and phase-space trajectories to play a similar diagnostic role. π states have been observed in ^{3}He-B, with outward spiraling phase-space trajectories.

An external drive ΔE, in the absence of damping, induces a running-phase state of rotation frequency related to ΔE. With damping, we find numerically that running-phase rota-

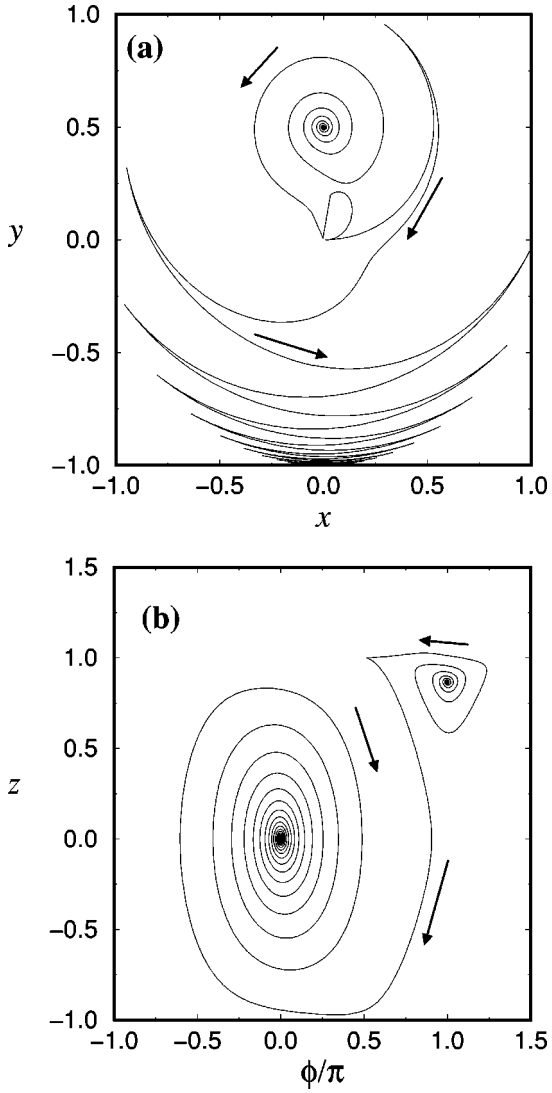

FIG. 5. (a) Coordinate-space trajectory for mode (D), and damping $\eta=0.05$; (b) phase-space trajectory of motion shown in (a).

tions decrease in amplitude to a final steady state of downward orientation ($\phi=0$) with zero angular velocity $\dot{\phi}=0$. There is a *nonzero* BEC population imbalance $z\neq 0$, in the steady state determined by setting $\phi=0$ in (3.1b), corresponding to a pendulum length $\sqrt{1-z^2}$ less than unity. By contrast, the damped SJJ with a nonzero external dc voltage reaches an ''ac Josephson'' steady state: the ac current and voltage are nonzero, corresponding to a (rigid-) pendulum rotation at average angular velocity $\langle\dot{\phi}\rangle\neq 0$.

Finally, we comment on the quantum version of the BJJ, and the regime in which the semiclassical treatment leading to the nonrigid pendulum is adequate. For the SJJ, with Cooper-pair number (difference) operator $\Delta\hat{N}$, the quantum regime is $E_c/E_J>1$, where $E_c(E_J)$ is the charging energy (coupling energy). For the BEC, the corresponding energies are U and $2KN_T$, determined by GPE matrix elements [5,6]. Thus, quantum fluctuations are important for $\Lambda\gg N_T^2$. This implies a wide regime [3], $\Lambda(N_T)<N_T^2$, where the semiclassical nonrigid-pendulum model for the BJJ is valid.

IV. CONCLUSIONS

Bose-Einstein condensate tunneling between double-well traps can be mapped onto a momentum-shortened nonrigid pendulum, with five distinct oscillation modes, that are all affected by damping in characteristic ways. Although they end up in the equilibrium rest state of zero pendulum tilt angle, their coordinate and phase-space trajectories are dynamical signatures of their original state of oscillation. In particular, inverted-pendulum π-oscillation states increase in amplitude due to damping, and undergo phase slips. Transitions between pendulum-rotation states of self-trapped BEC population, and pendulum oscillation states, show singular dips in inverse periods as the pendulum mass is changed, that are still distinguishable for low enough dampings/temperatures. These damped nonrigid-pendulum dynamical states could be observable in double-well BEC traps; ^{3}He-B pair tunneling through micropores; and transitions between different hyperfine states in harmonic traps.

ACKNOWLEDGMENT

S.R. acknowledges the support of NSF Grant No. PHY94-15583.

[1] M. H. Anderson, J. R. Ensher, M. R. Mathews, C. E. Wieman, and E. A. Cornell, Science **269**, 198 (1995); K. B. Davis, M. O. Mewes, M. R. Andrews, N. J. van Druten, D. S. Durfee, D. M. Kurn, and W. Ketterle, Phys. Rev. Lett. **75**, 3969 (1995); C. C. Bradley, C. A. Sackett, J. J. Tollett, and R. G. Hulet, *ibid.* **75**, 1687 (1995); D. G. Fried, T. C. Killian, L. Willmann, D. L. Landhuis, S. C. Moss, D. Kleppner, and T. J. Greytak, *ibid.* **81**, 3811 (1998).

[2] F. Dalfovo, S. Giorgini, L. P. Pitaevskii, and S. Stringari, e-print cond-mat/9806038; A. S. Parkins and D. F. Walls, Phys. Rep. **303**, 1 (1998).

[3] J. Javanainen, Phys. Rev. Lett. **57**, 3164 (1986); G. J. Milburn, J. Corney, E. M. Wright, and D. F. Walls, Phys. Rev. A **55**, 4318 (1997).

[4] I. Zapata, F. Sols, and A. J. Leggett, Phys. Rev. A **57**, R28 (1998); F. Sols, e-print cond-mat/9810338.

[5] A. Smerzi, S. Fantoni, S. Giovanazzi, and S. R. Shenoy, Phys. Rev. Lett. **79**, 4950 (1997).

[6] S. Raghavan, A. Smerzi, S. Fantoni, and S. R. Shenoy, Phys. Rev. A **59**, 620 (1999).

[7] J. Ruostekoski and D. F. Walls, Phys. Rev. A **58**, R50 (1998).

[8] J. Williams, R. Walser, J. Cooper, E. Cornell, and M. Holland, Phys. Rev. A **59**, R31 (1999).

[9] A. Smerzi, S. Raghavan, S. Fantoni, and S. R. Shenoy (unpublished).

[10] B. P. Anderson and M. A. Kasevich, Science **282**, 1686 (1998).

[11] S. V. Pereverzev, A. Loshak, S. Backhaus, J. C. Davis, and R. E. Packard, Nature (London) **388**, 449 (1997); S. Backhaus, S. V. Pereverzev, A. Loshak, J. C. Davis, and R. E. Packard, Science **278**, 1435 (1997); S. Backhaus, S. V. Pereverzev, R. W. Simmonds, A. Loshak, J. C. Davis, and R. E. Packard, Nature (London) **393**, 687 (1998).

[12] T. A. Fulton, in *Superconductor Applications*, edited by B. Schwarz and S. Fower (Plenum, New York, 1976), Chap. 4.

[13] A. Barone and B. Paterno, *Physics and Applications of the Josephson Effect* (Wiley, New York, 1982).

[14] R. P. Feynman, R. B. Leighton, and M. Sands, *The Feynman Lectures on Physics* (Addison-Wesley, Reading, MA, 1963).

[15] H. Ohta, in *SQUID: Superconducting Quantum Devices and their Applications*, edited by H. D. Hahlbohm and K. Lubbig (de Gruyter, Berlin, 1997).

[16] A. Narayanan, A. Smerzi, S. Raghavan, S. Fantoni, and S.R. Shenoy (unpublished).